IEEE Access
Multidisciplinary ⋮ Rapid Review ⋮ Open Access Journal

Received July 24, 2020, accepted July 30, 2020, date of publication August 3, 2020, date of current version August 17, 2020.

Digital Object Identifier 10.1109/ACCESS.2020.3013901

Evaluating Angularity of Coarse Aggregates Using the Virtual Cutting Method Based on 3D Point Cloud Images

HANYE LIU[1,2], (Member, IEEE), ZHAOYUN SUN[1], WEI LI[1], JU HUYAN[3], MENG GUO[4], AND XUELI HAO[1]

[1]School of Information Engineering, Chang'an University, Xi'an 710064, China
[2]School of Information Engineering, Yulin University, Yulin 719000, China
[3]Department of Civil and Environmental Engineering, University of Waterloo, Waterloo, ON N2L 3G1, Canada
[4]Key Laboratory of Urban Security and Disaster Engineering of Ministry of Education, Beijing University of Technology, Beijing 100124, China

Corresponding authors: Zhaoyun Sun (zhaoyunsun@126.com) and Wei Li (235240274@qq.com)

This work was supported in part by the National Natural Science Foundation of China under Grant 51868076 and Grant 51908059, in part the Key Research and Development project of Shaanxi Province, China, under Grant 2018GY-024, in part by the Natural Science Basic Research Program of Shaanxi Province, China, under Grant 2017JQ5014, in part by the Fundamental Research Funds for the Central Universities under Grant 310824171005, and in part by the Key Laboratory of Highway Engineering in Special Regions.

ABSTRACT In this paper, a new method called the Virtual Cutting Method is proposed to evaluate the angularity index (AI) values of 3D point cloud coarse aggregate images with the aim of characterizing the angularity of aggregates on conveyor belts. The 3D point cloud images of coarse aggregates were first captured, preprocessed, and segmented into single 3D aggregate objects. Based on the processed 3D aggregate images, intersection contours were extracted using a series of intersection planes with an equivalent angle between two adjacent planes. The AI was evaluated by averaging the angularity of the contours using the gradient method, which was used in the AIMS2 system. Statistical analysis was then performed to select the optimum angle between two adjacent planes. It was found that an angle of five degrees was the ideal angle, as it can balance the execution time and effectiveness of the method. Finally, the AI results of the Virtual Cutting Method were compared with those of 2D and 3D Projection Methods. It was found that the AI rankings of the three methods for different aggregate textures are generally consistent. The findings of this study conclude that the Virtual Cutting Method can be employed to quantify the angularity of a single aggregate or aggregates in piles on conveyor belts based on 3D point cloud images.

INDEX TERMS Aggregate particles, angularity evaluation, 3D point cloud image, virtual cutting.

I. INTRODUCTION

As one of the most important ingredients of construction materials in both asphalt concrete and hydraulic cement concrete, the morphological characteristics of aggregates, including the shape, angularity and texture (Figure 1), significantly affect the performance of pavement systems [1]–[4]. As shown in Figure 1, coarse aggregate angularity is defined as the sharpness of corners/nicks and can improve the shear strength properties of hot-mix asphalt (HMA) and unbound aggregate base layers [5]–[7]. Pavement performance indicators affected by aggregate angularity include the dosage of binder, dynamic modulus, high-temperature stability, and microstructure characteristics [7], [8]. To guarantee the critical performance of the pavement, the particle angularity should be well assessed.

Currently, in a pavement management system, the measurement of aggregate angularity is mainly based on human operation and the operators' experience, which is criticized as tedious, time-consuming, and subjective [8], [9]. With the development of the machine vision technique, image analysis has been used extensively to characterize the size and shape of aggregate or gravel particles on conveyor belts in the aggregate industry [10]–[18]. However, due to harsh industrial environments in the aggregates industry, such as poor light conditions and excessive dust in the air, the 2D or 3D imaging method (camera) may not capture high-quality images (e.g., shadows from objects). In addition, the aggregates on

The associate editor coordinating the review of this manuscript and approving it for publication was Mehul S. Raval.

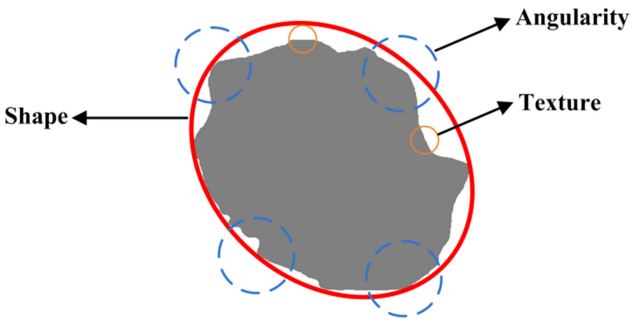

FIGURE 1. Morphological characteristics of aggregates.

conveyor belts are often in piles, and the surface aggregates of piles can be entirely or partially visible (See Figure 2.). Even if the aggregates are in monolayer, the angularity of touched aggregates cannot be effectively evaluated using traditional projection methods.

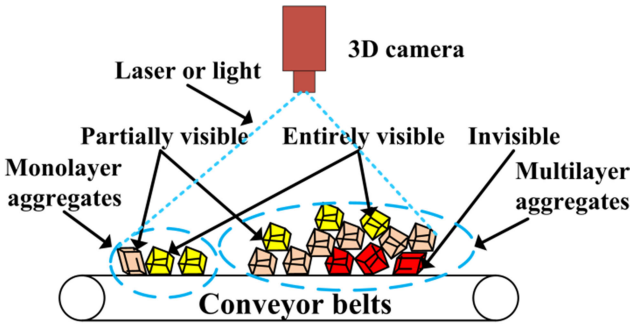

FIGURE 2. Aggregates on conveyor belts. Left, monolayer aggregates; right: multilayer aggregates. When a 3D camera projects laser or light on the aggregates, only the entirely visible and partially visible aggregates can be scanned.

Furthermore, a literature review related to the angularity evaluation of coarse aggregates reveals that most of the current image-based systems for measurement of aggregate angularity in a laboratory, as well as test samples of aggregates, should be prepared and placed properly. Upon comparison with the sampling tests in a laboratory, on-site analysis on conveyor belts can accommodate more samples for testing, and can also provide real-time feedback for mine and quarry operators. The real-time feedback not only helps to improve the quality of aggregates, but can also reduce the costs of the quarrying operation. Figure 3 shows a schematic overview of the workflow of an aggregate plant using a machine vision system for measuring aggregate angularity index.

Because of the direct measurement of the surface point height for the laser scanning images (point cloud or range images), the scanning method can overcome the problem of shadows obscuring the surface data. However, only the top surface points can be captured using the laser scanning camera. Thus, the 3D projection method may not evaluate the AI of aggregates effectively because of the lack of partial 3D information. In addition, when the aggregates are arranged in piles (Figure 2.), even 2D projection profile images of some top-surface particles of aggregate piles can be obtained correctly when multiple aggregates overlapped. To address the AI of particles on conveyor belts, a new method (referred to as ''Virtual Cutting Method'') is proposed to evaluate the angularity of the surface aggregates based on point cloud images.

In summary, the proposed AI evaluation method makes the following contributions:

a) a new method of evaluating AI of coarse aggregates that uses the gradient method (used in AIMS2 system) to evaluate the AI of a series of intersection lines between the cutting planes and 3D object, in which the AI of the aggregates was calculated by averaging all the AI of intersection lines; and

b) exploration of best cutting degrees for aggregates of different sizes and textures.

II. RELATED WORK

A. 3D POINT CLOUD ACQUISITION METHOD

3D point data obtained from sensing technologies can be used to reconstruct the 3D surface geometries of target objects in an accurate and efficient manner. Light Detection and Ranging (LiDAR), structure light technology, stereo cameras, and photogrammetry are commonly used sensing methods [19], [20]. LiDAR is a laser scanning technique that can collect the 3D XYZ position data of each scanned point by measuring properties of reflected light to determine distance to a target. The structure light technique utilizes a projection device to project structured patterns onto the object, a camera captures the distorted structured images and then the 3D coordinate values can be constructed [20]. A stereo camera uses two or more cameras to infer depth by means of triangulation based on the corresponding points in the captured images [21]. Photogrammetry generates point cloud data based on a collection of overlapping images of the target object.

For the 3D measurement of aggregates on conveyor belts, 3D sensing technologies were able to achieve high performance in terms of speed and accuracy. For the image-based methods stereo camera, and photogrammetry, their centimeter-level accuracies make them unsuitable for measuring the coarse aggregates of size in the range of a few millimeters to a few centimeters [19]. Furthermore, a stereo system has limitations for real-life applications due to its considerable computational expense, which hinders its wide use in real-time measurements on conveyor belts. For range-based methods, that is, ground LiDAR (also known as terrestrial laser scanning) and structure light technology, the surface of the object was scanned by laser or a stripe of light directly, and then the distance was determined based on the known relative positions of the light source and optical sensor [22], [23]. Because of this feature, the two methods can provide accurate and complete details with a high degree of

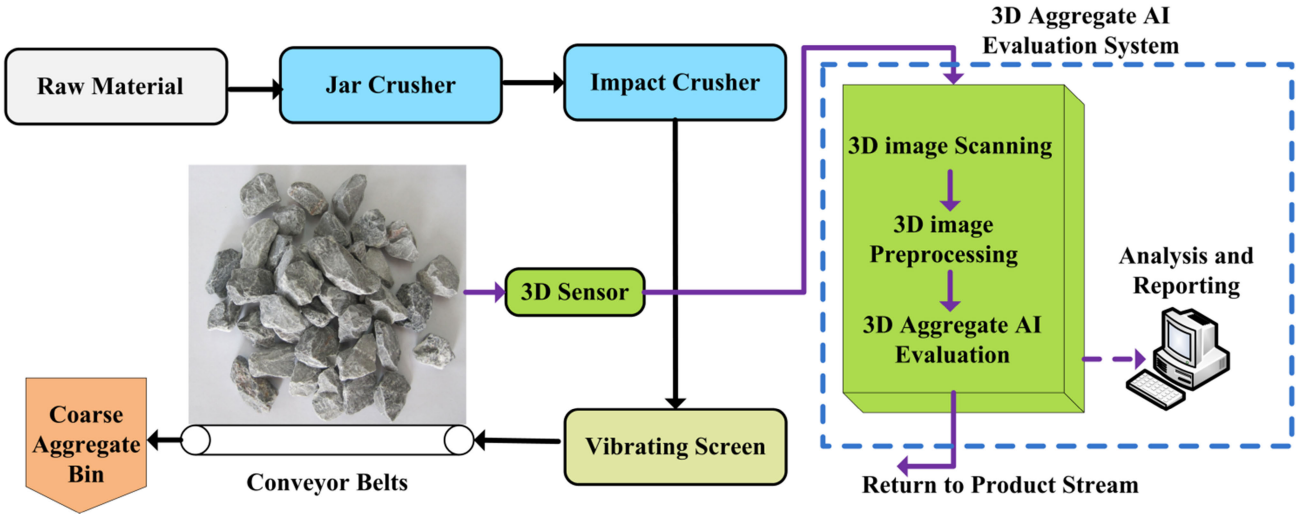

FIGURE 3. Schematic overview of system for measuring aggregate angularity index in a coarse aggregate plant [25]. Production flow consists of four major processes: primary crushing, secondary crushing, screening and transporting to aggregate bin by conveyor belts. The 3D aggregate AI evaluation system has three main function modules: 3D image scanning, 3D image preprocessing, and aggregate AI evaluation; 3D aggregate images were captured from conveyor belts.

automation, and accurate geometric information of the object can be obtained. In addition, the structure light system with a single camera has the shortcoming of camera occlusion [24]. For these reasons, a 3D structure light device with dual cameras was used in this research.

B. AGGREGATE ANGULARITY EVALUATION METHOD

In recent decades, various image analysis methods that analyze 2D or 3D images acquired via different means (apparatus) have been used to evaluate aggregate angularity [26] including 2D imaging (camera), X-ray (computed tomography scanner), 3D images, and laser scanning (laser scanner).

2D angularity descriptors based on 2D variables in spatial and frequency domains are determined through image analysis of particle projections [1], [2], [27]–[32]. The aggregate imaging measurement system 2 (AIMS2) is a commercialized imaging system based on the gradient method and is used to evaluate aggregate angularity, which has proven effective for angularity characterization [9], [33], [34]. Wang [35] implemented a unified Fourier Morphological Analysis Method to evaluate aggregate angularity as described by the intermediate portions of the Fourier series of particle profiles.

X rays can be used to obtain photographs at different cross-sections of the particles, and there have been some studies utilizing this technique to evaluate the shape of aggregates [36]–[39]. Yang *et al.* [40] used the '3D Sobel-Feldman Operation' to determine the angularity index (AI); the results showed that the method could determine the 3D AI of aggregates. Erdogan *et al.* [41] showed that spherical harmonic analysis was suitable for the shape of the coarse aggregates' X-ray images.

3D images utilize the projected images from different views to reconstruct the 3D image [26]. The University of Illinois Aggregate Image Analyzer (UIAIA) is another commercialized imaging system based on tracing the change in the slope of the particle image outline obtained from each of the top, side, and front images. A final AI is then established by taking a weighted average of the AI for all three views [5], [42]. Tong *et al.* [8] designed a 3D CNN network to evaluate aggregate angularity based on the images from three cameras in different directions, the results showed that it was very robust under different light conditions, sizes and aggregate textures. The Laser Scanning Method determines the 3D coordinates of the surface points and can be used to obtain 3D images [26]. Kim *et al.* [43] proposed a wavelet-based 3D particle shape descriptor for stone aggregates that showed a strong correlation with human visual perceptions. Lee *et al.* [44] evaluated aggregate angularity via particle shape interpretation.

Although the above methods can evaluate aggregate angularity, shortcomings of the existing strategies remain as follows: (1) the 2D AI was based on projected images, which could not completely reflect the aggregate angularity [8]; (2) most of the proposed angularity characterization methods were used for laboratory tests on sample aggregates and thus may not be suitable for real-time AI calculation of aggregates on conveyor belts [5], [9], [26], [33], [34], [42]; and (3) the X ray-CT scanning and post-processing time was long, which was not suitable for real-time processing [26]. Thus, a comprehensive evaluation of the 3D angularity method for aggregates on conveyor belts is required.

III. THE PROPOSED SOLUTION

Figure 4 shows the research procedure used in this paper. The 3D point cloud images of aggregate particles were captured

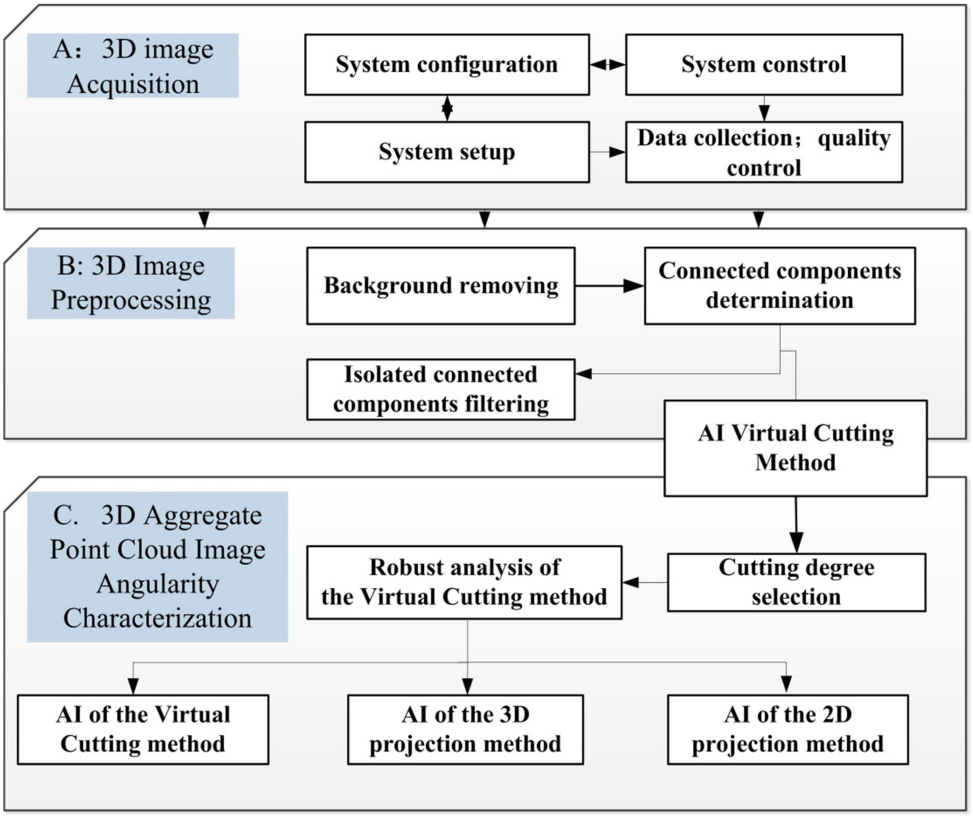

FIGURE 4. Flowchart of research procedure, which consists of 3D image acquisition, 3D image preprocessing and 3D aggregate point cloud image angularity characterization. Validity of the method was verified by comparison with 2D/3D projection methods.

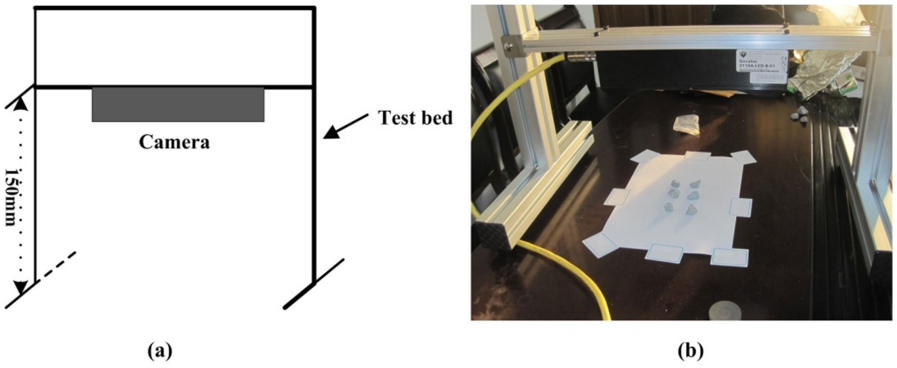

FIGURE 5. Illustration of image-acquisition system: (a) schematic of custom testbed; (b) 3D cloud point image acquisition system.

via a binocular vision system. The preprocessing stage consisted of background removal and aggregate segmentation. The Virtual Cutting method is proposed to evaluate the AI of coarse aggregates based on contours extracted from the intersection of a series of planes and the 3D aggregate objects. Because the lower cutting degree between two adjacent cutting planes may take too much execution time, statistical analysis was used to determine the optimal cutting degree. Finally, the robustness of the method was discussed by comparing with the 2D/3D projection method.

A. 3D IMAGE ACQUISITION

A self-developed device (Test Bed) was used to acquire aggregate cloud point images, as shown in Figure 5. From Figure 5, a 3D binocular camera (Gocator 3110) with a blue LED was mounted horizontally on the test-bed. The height of the camera could be manually adjusted based on the required field of view(FOV) and the distance between the camera and the surface of the desk was covered with the white paper (about 150 mm). In our experiment, the FOV width, height and depth were 100 mm, 170 mm, and 100 mm, respectively.

After camera calibration, the resolution along the X, Y and Z axes were 0.5, 0.5, and 0.35 mm, respectively. In addition, a 16-bit format was used for the captured images, where the height map, intensity, and stamps are stored in the red, green, and blue channels, respectively. Each captured PNG image is 201∗341 pixels.

B. 3D IMAGE PREPROCESSING

The first step in this stage is to extract the heightmap, intensity and stamp information from the captured PNG images for constructing the 3D point cloud images in a subsequent stage. Based on the three images, a 3D model was constructed (Figure 6.). As illustrated in Figure 6(a), the 3D image contains many noisy points (Z-Coordinates with very small values), which can be regarded as the background image and can be removed by the threshold method based on the Z-Coordinates. The 3D aggregate particle segmentation process was as follows:

Step 1: Background removing. The background image was removed by selecting the 3D points whose Z-Coordinates were in the range specified by minimum and maximum values. The minimum and maximum values were set to 0.5 and 100, respectively.

Step 2: Determine the connected components of the 3D object model. The connected components were determined by measuring the distance between the pixel coordinates of points in the 3D object model that were stored in 2D mapping, the value was set to 2.

Step 3: Remove the connected components that have a smaller number of points. After step 2, some connected components that have a smaller number of points may exist. These components are not the aggregate particles and should, therefore, be removed before the next iteration. The connected components were regarded as a valid component if the number of points was greater than 100.

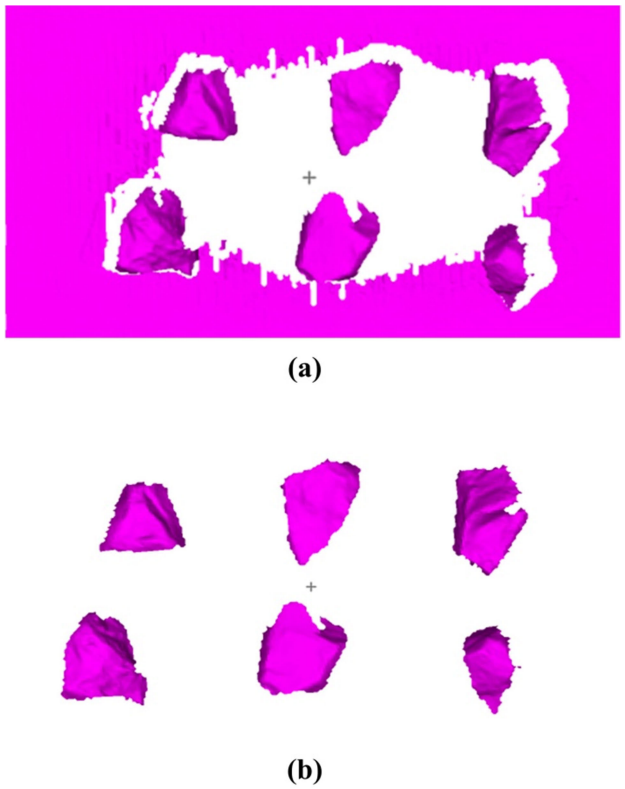

FIGURE 6. Aggregate image preprocessing and segmentation: (a) raw 3D image; (b) segmented 3D image after background removal, connected component determination, and small component removal.

C. 3D AGGREGATE POINT CLOUD IMAGE ANGULARITY CHARACTERIZATION

For aggregate angularity characterization, the gradient-based approach in the Aggregate Image System (AIMS) has been proven as an effective method [9]. The concept behind the gradient-based approach is to calculate the changes in gradient vectors of points on an edge profile (Figure 7.). In the current research, based on the gradient-based approach, two methods (the projection method and the virtual cutting method) were employed to extract the edge profiles, to evaluate the angularity of 3D point cloud aggregate particles.

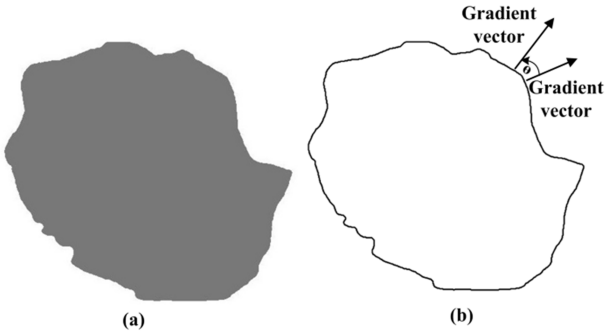

FIGURE 7. Illustration of gradient approach: (a) silhouette of aggregate particle; (b) gradient method based on contour of aggregate silhouette.

1) DESCRIPTION OF THE GRADIENT APPROACH

The gradient approach used in AIMS is analyzed by quantifying the change in the gradient on a particle boundary. The gradient approach starts by calculating the direction of the gradient vectors on particle boundary points from the X-axis (horizontal axis in an image). The average change in the direction of the gradient vectors is taken as follows [27]:

$$\text{AI (GradientApproach)} = \sum_{i=1}^{N-3} |\Theta_i - \Theta_{i+3}| \qquad (1)$$

where the subscript i denotes the ith point on the boundary of a particle, and N is the total number of points on the boundary. The steps to calculate the AI using the gradient approach are as follows:

Step 1: Obtain the contour point of the aggregate particle. The number of contour points was counted. If the number of contour points was less than 4, the angularity of the extracted contour could not be obtained and was ignored.

Step 2: Calculate the gradient vector of the particle boundary points. The gradient of an image f(x, y) at the location

(x, y) is taken as follows [27]:

$$\mathrm{f} = \begin{pmatrix} \mathrm{G_x} \\ \mathrm{G_y} \end{pmatrix} = \begin{bmatrix} \frac{\partial f}{\partial x} \\ \frac{\partial f}{\partial y} \end{bmatrix} \tag{2}$$

Step 3: Calculate the direction of the gradient vector represented by the angle vector $\theta(x, y)$ of the gradient vector at the location (x, y). The angle vector is taken as follows [27]:

$$\theta\,(\mathrm{x}, \mathrm{y}) = \tan^{-1}\left(\frac{G_x}{G_y}\right) \tag{3}$$

Step 4: Calculate the angularity using formula (1).

2) ANGULARITY ANALYSIS BASED ON PROJECTED IMAGES

In the 3D angularity characterization of coarse aggregates, the view method, which uses single or multiple views for 3D object reconstruction, is often used [8], [45]. The view images can be obtained from a group of cameras; this is often three cameras located at the front, top, and side [46]. The angularity is calculated based on these different view images. For the 3D cloud image of coarse aggregates, if the position of the XY, YZ and XZ planes are determined in the XYZ coordinate system, the projected images on the three planes can be obtained under internal camera parameters. Thus, after the contour of the projection images are extracted, the angularity can be calculated by the gradient method. The steps to evaluate the angularity based on the projection images are as follows:

Step 1: The intrinsic and extrinsic camera parameters were determined for the projected images. The internal camera parameters can be obtained using the built-in calibration software. The extrinsic camera parameters define the geometric transformation (translation and rotation) between the camera frame, relative to the scene coordinate frame. Three 3D pose vectors based on extrinsic camera parameters were constructed in the experiment in order to obtain the three projection images onto the XY, YZ and XZ planes in the XYZ coordinate system. The 3D pose, which is the so-called rigid transformation, includes a translation vector and a rotation matrix [47]. The translation vector includes 3 parameters: TransX, TransY, and TransZ, which specify the translation along the X, Y and Z axis, respectively. The rotation matrix, which can also be described as 3 parameters, RotX, RotY, and RotZ, specify the rotation along the X, Y and Z axis, respectively. If the internal camera parameter is determined, a projection depth image can be obtained, combined with a 3D pose. A 6D vector P is used to represent the pose vector consisting of translation vector and rotation by setting P = [TransX, TransY, TransZ, RotX, RotY, RotZ]. It is conceivable that the difference between the three poses exists among the rotation vectors, and the translation vectors are the same. The pose vector $\mathrm{P_{xy}}$ used to project the projection image on the XY plane was set to [0, 0, 0, 0, 0, 0]. The pose vector $\mathrm{P_{yz}}$ used to project the projection image on the YZ plane was set to [0, 0, 0, 0, −90, 0]. The pose vector $\mathrm{P_{xz}}$ used to project the projection image on the XZ plane was set to [0, 0, 0, 90, 0, 0].

Step 2: Project the 3D aggregate point image onto the XY, YZ and XZ planes in the XYZ coordinate system. Based on the 3D pose and internal camera parameters, a projection matrix can be constructed. Thus, under perspective projection, the projection point can be obtained via the rank-3 projection matrix H and a 3D input point x as $\mathrm{P_p} = \mathrm{H}\hat{\mathrm{X}}$, where $\hat{\mathrm{X}} = \left[\mathrm{X^T}, 1\right]^{\mathrm{T}}$ is the homogeneous form of point x and $\mathrm{P_p}$ is the projection point. Figure 8(b) shows the three projection images.

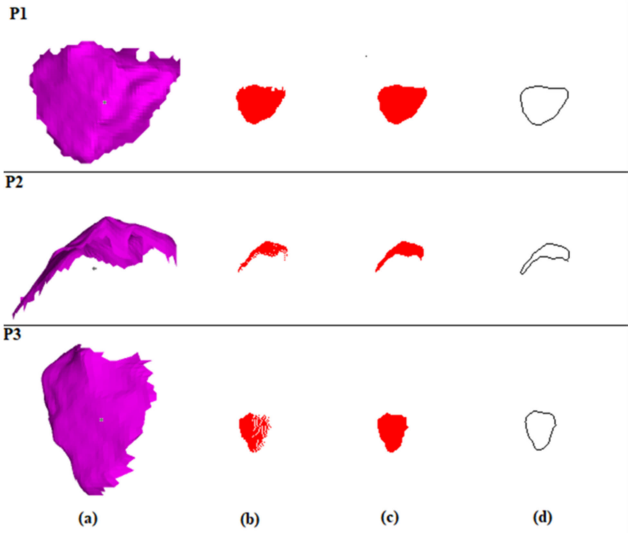

FIGURE 8. Projection of aggregate image on XY (P1), YZ (P2) and XZ planes (P3) in XYZ coordinate system: (a) magnified 3D aggregate object viewed from direction of Z, X and Y axes in XYZ coordinate system; (b) preprocessed projected images on the three planes in XYZ coordinate system; (c) projection images after morphological closing operation; (d) contours of projected images.

Step 3: Close the projection region using a circular structuring element. It can be observed in Figure 4 that the projected images (Figure 8 (b)) onto the XY, YZ and XZ planes are not smooth at the edges or internal regions, and the problem was more serious on the projected images of the YZ and XZ planes. Thus, a close operation of a circular structuring element was completed on the projection image. Figure 8 (c) shows the images after processing. The radius of the circular structuring element was set to 5.5 in the present work.

Step 4: Extract the contour of the three projection images. Figure 8(d) shows the contour image.

Step 5: Calculate the AI using the contour of the three projected images based on the gradient method shown in formula (1). In the present work, two methods (2D projection and 3D projection methods) were proposed to evaluate the AI of aggregates based on projected images. The 2D projection method calculates the AI based on the contour of the projection image on the XY plane, and the 3D projection method calculates the AI by adding the three angularity indices, taken as follows:

$$\mathrm{AI}_{2d} = \mathrm{AI}_{pxy} \tag{4}$$

$$\mathrm{AI}_{3d} = \mathrm{AI}_{pxy} + \mathrm{AI}_{pxz} + \mathrm{AI}_{pyz} \tag{5}$$

where pxy, pxz, and pyz are the contours of the three projected images on the XY, YZ and XZ planes, respectively, in the XYZ coordinate system. AI_{2d} and AI_{3d} represent the AI of the 2D projection method and 3D projection method, respectively.

3) ANGULARITY ANALYSIS BASED ON THE VIRTUAL CUTTING METHOD

The 3D acquisition equipment employed, Gocator 3110, is a kind of snapshot sensor (captures an entire surface in a single snapshot). The camera works by projecting several structured light patterns in a rapid sequence onto the target. The point cloud data can be obtained when the reflection of the pattern of the target is captured by two cameras [48]. If the reflection of the pattern of the target cannot be captured by the cameras, such as the captured surface in a perpendicular direction to the reference plane or beneath the top surface, the 3D point cloud data cannot be obtained. To illustrate the limitation of the projection method for angularity evaluation of aggregates based on the structure light technique, a capsule-shaped object, which consists of three parts, a blue half ellipsoid (top surface), orange cuboid (vertical surface) and orange half ellipsoid (beneath the top surface), was constructed (Figure 9). It is evident that only the 3D point data of the top surface (blue half ellipsoid) can be obtained, as the light patterns cannot be projected onto the vertical surface and that beneath the top surface. Figure 10 shows the projected image contour of the captured object on the XY, YZ and XZ planes in the XYZ coordinate system. The projected contour on the planes XZ and YZ contains fake edges (the red line) that may influence the accuracy of the angularity characterization.

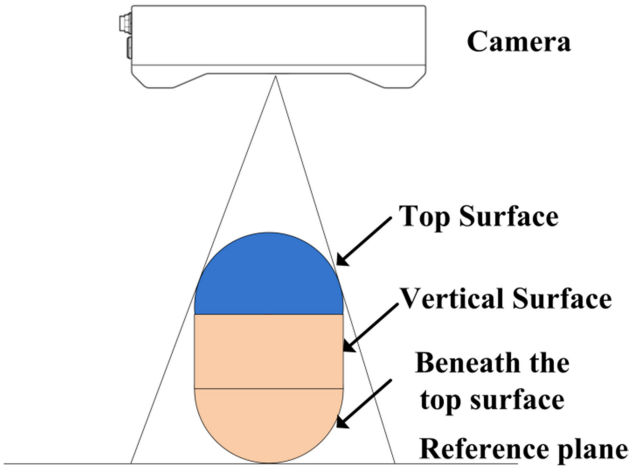

FIGURE 9. Illustration of 3D point cloud image acquisition for capsule-shaped object. Only the top surface of the object can be captured because of the occlusion problem in the 3D structure light system.

To address the problem of evaluating the AI of aggregates based on the 3D points of its top surface on conveyor belts, the Virtual Cutting Method is presented in this research. We use the term ''Virtual Cutting'' because the intersection line used to evaluate the AI of the aggregates obtained by the intersection of the aggregate 3D model and a plane, just as a virtual knife cuts a 3D aggregate object. For aggregates on conveyor belts, the aggregates may be in piles; thus, traditional AI evaluation methods based on the 2D projection contour may not work correctly, because part of the particle may be hidden beneath other particles. The major advantage of the proposed method is that it uses the 3D point data of the aggregates' top surfaces, irrespective of touched or separated aggregates on conveyor belts.

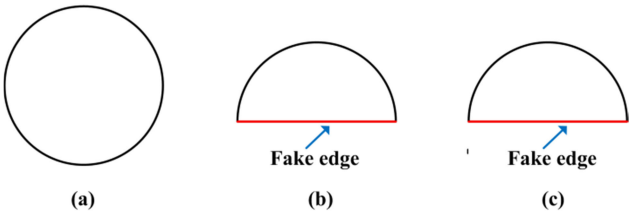

FIGURE 10. Contours of three projected images for capsule-shaped object (Figure 9) in XYZ coordinate system (red parts are fake edges): (a) projection images on (a) XY, (b) YZ, and (c) XZ planes.

The principle of the Virtual Cutting Method is that an intersection between the aggregate 3D model and a plane was calculated, and the angularity was measured based on the cross-section line using the gradient method discussed in section 2.2.1. The principle diagram of the 3D model intersection of the plane is shown in Figure 11. As illustrated in Figure 11, three parallel planes, known as Planes A, B, and C, pass through the aggregate 3D model and are perpendicular to the XY projection plane in the XYZ coordinate system. The angle between Planes A and B is 30 degrees, and the angle between Planes B and C is 110 degrees. Figure 12 shows the intersection contour of the cross-section between the plane and the 3D object. As shown in Figure 12, the three contour images are different, especially for Figure 12(c) and the other two images (Figures. 12(a) and (b)). With these contours, the angularity can be measured using the gradient method discussed in section 2.2.1. The steps to evaluate the angularity based on the Virtual Cutting Method are as follows:

Step 1: Create a surface triangulation for the 3D object model. The captured aggregate 3D models were represented

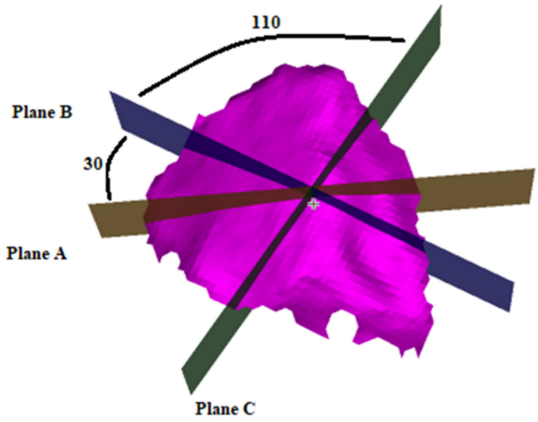

FIGURE 11. Illustration of Virtual Cutting Method. Three parallel planes (A, B and C) pass through aggregate 3D mode. The three intersection lines were extracted for AI evaluation for aggregates.

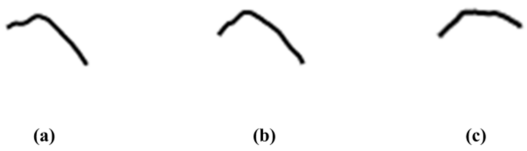

FIGURE 12. Intersection contours between 3D aggregate object and cutting plane mentioned in FIGURE 11: contours extracted using planes (a) A, (b) B, and (c) C.

as 3D point clouds, and the surface model was triangulated in many cases to obtain accurate 3D point clouds [49].

Step 2: Determine the center coordinate of the aggregate 3D object. As shown in Figure 10, the intersection plane passes through the center coordinate point of the 3D object. Thus, the center coordinate of the aggregate 3D object should be calculated to further determine the intersection plane pose.

Step 3: Determine the pose of the intersection plane. The pose vector of the first intersection plane was set to [$Center_{Cx}$, $Center_{Cy}$, $Center_{Cz}$, 0, 90, 0], where $Center_{Cx}$, $Center_{Cy}$, and $Center_{Cz}$ are the center coordinates of the aggregate 3D object, and the last three components [0, 90, 0] depict that the plane through the center of the 3D object is parallel to the XY plane, which is rotated 90 degrees along the Y-axis in the XYZ coordinate system. The pose of the other intersection planes is set to [$Center_{Cx}$, $Center_{Cy}$, $Center_{Cz}$, 0, 90, θ_{step}], where θ_{step} is a value in a sequence of equidistant values with a given step within the range of the step and 180 degrees. For instance, if the step is 30, the θ_{step} is a value in the sequence vector [0, 30, 60, 90, 120, 150, 180].

Step 4: Intersect the 3D object model with the intersection plane. The Halcon operator 'intersect_plane_object_model _3d' [50] was used to extract the 3D intersection line of the cross-section through the intersection plane that is defined by the pose mentioned in Step 3. To calculate the angularity of the 3D intersection line, it should be projected as a 2D image.

Step 5: Project the 3D intersection line into a 2D contour line.

Step 6: Calculate the AI for the projected contour using the gradient method.

Step 7: Calculate the aggregate angularity based on the AI of the projected contours. In the present work, the aggregate angularity was calculated by averaging the AI of the projected contours taken as follows:

$$\text{AI} = \frac{\sum_{i=1}^{n} \text{AI}_{\text{Pc}}}{n} \tag{6}$$

where Pc is the projected contour, and n is the number of projected contours.

IV. RESULTS AND DISCUSSION

A. PERFORMANCE OF THE VIRTUAL CUTTING METHOD

As previously discussed, the intersection contour was extracted based on a series of adjacent cutting planes, and the angle degrees between the adjacent cutting planes were set to a fixed value. It is conceivable that the greater the angle value selected, the fewer intersection contours extracted. If the angle degree is too small, the extracted intersection contours might not be enough to characterize the aggregate 3D model. Moreover, if the angle degree is too large, it might take a long time to implement the intersection contour extraction. Thus, a proper angle degree needs to be determined, which would keep a balance between the effective angularity characterization and the system run time. In the current research, eight different angle degrees were selected, including 1, 3, 5, 10, 15, 20, 25 and 30 degrees.

1) DIFFERENT ANGLE DEGREES ANALYZED WITH DIFFERENT AGGREGATES SIZES

For the purpose of verifying the robustness of the angularity characterization based on the virtual cutting method at different angles for different sizes of aggregates, gneiss aggregate particles with different sieve sizes (9.5–13.2, 13.2–16, and 16–19 mm) were sieved with square apertures manually. The numbers of the aggregate particles were 187, 160, and 198, respectively. Eight different angles were used to implement virtual cutting. Box plots (left) with data scatter plot (right) were adopted to analyze the AI values. The AI results of the three sieve-size aggregate particles are shown in Figure 13. As shown in Figure 13(a), for the aggregates with sizes of 9.5–13.2 mm, the shape of the AI box plot for angle degrees of 1, 3, 5, 10, 15, and 25 were close to each other, and the results of 20 and 30-degree angles were different compared to the others in terms of the shape of the box plots. For the aggregates with sizes, 13.2–16 mm, the shape of the AI box plot for angle degrees of 1, 3, 5, 10, 15, 20, and 25 were close to each other, and the results of the 30-degree angle were different from the others in terms of the shape of the box plots. For the aggregates with sizes, 16–19 mm, the shape of the AI box plot for the angle degrees of 1, 3, 5, 10, 15, and 30 were very close to each other, and the results of 20 and 25 degrees were noticeably different from others in terms of the shape of the box plots. These results indicate that the AIs of aggregates with different sizes were stable when the cutting angle was less than 15°.

The 1st and 3rd quartile range values of the box plots for the AI with different sieve sizes (9.5–13.2, 13.2–16, and 16–19 mm) are shown in Table 1. Just like the shape for the AI box plot under different cutting degrees, the 1st and 3rd quartile range values of the box plots for the AI of aggregates with different sizes with cutting angle degrees of 1, 3, 5, and 10 are also very close. The main reason for this was that when the cutting angle was less than 15°, the key parts of the aggregates' top surfaces represented the angularity of the aggregates that could be sampled adequately. In addition, the smaller the cutting angle, the more intersection contours could be extracted, and thus the greater chance of sampling the key parts of the aggregates that could represent its angularity; thus, more accurate AI results. Therefore, the AI value obtained by cutting with 1-degree may be the most accurate. However, the extraction of too many intersection contours

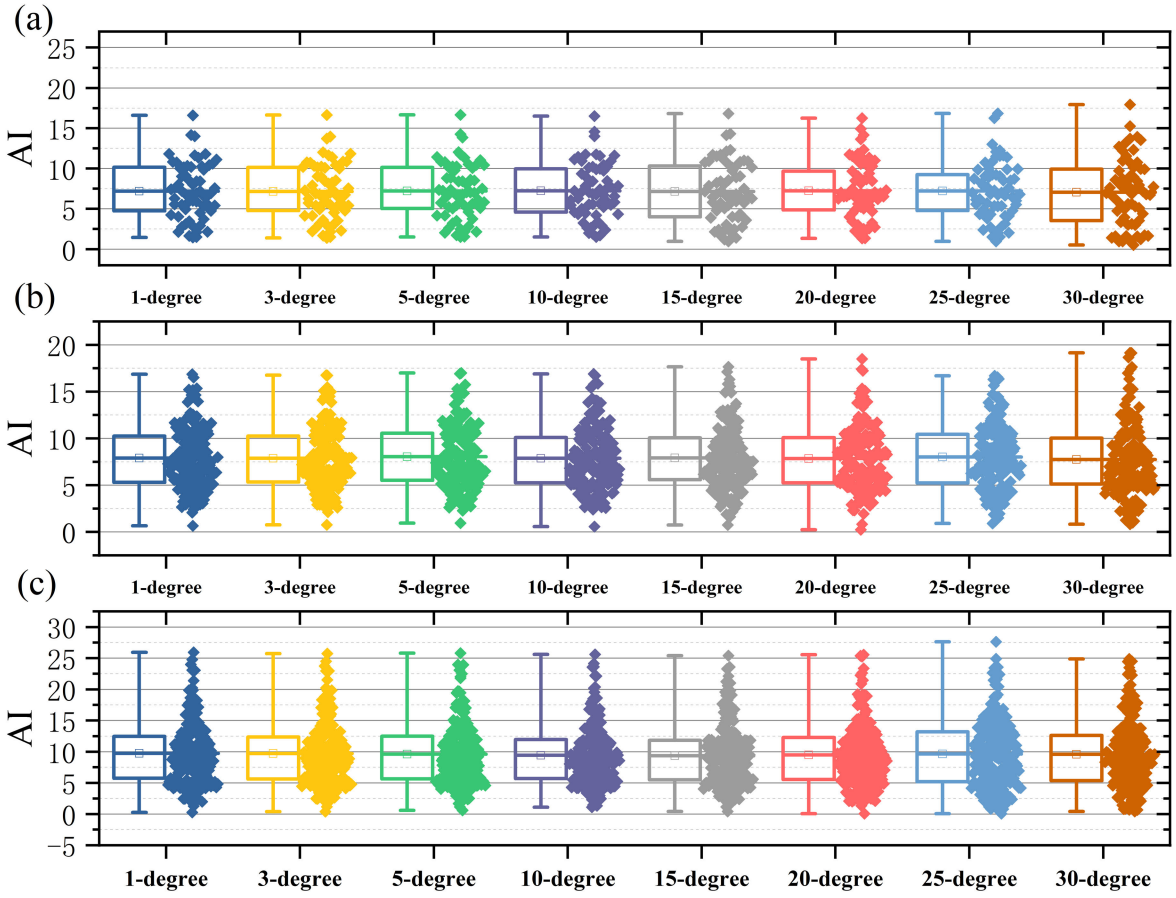

FIGURE 13. Box plots of AI for different sieve sizes of aggregates using Virtual Cutting Method: AI for sieve sizes of (a) 9.5–13.2 mm, (b) 13.2–16 mm, and (c)16–19 mm.

TABLE 1. AI ranges within first and third quartile ranges of aggregates with different sieve sizes using different cutting degrees.

Cutting degrees	Size 9.5–13.2 (mm)	Size 13.2–16 (mm)	Size 16–19 (mm)
1	4.91–10.09	5.37–10.61	5.74–12.45
3	4.89–10.08	5.36–10.55	5.64–12.35
5	4.80–10.07	5.56–10.66	5.66–12.46
10	4.97–9.96	5.26–10.30	5.71–11.95
15	4.68–10.16	5.58–10.58	5.50–11.83
20	4.78–9.84	5.26–10.41	5.58–12.25
25	4.80–10.07	5.32–10.85	5.21–13.16
30	4.46–10.31	5.15–10.64	5.40–12.59

may be time-consuming. Therefore, a scientific and reasonable choice of cutting degrees is imperative.

2) DIFFERENT ANGLE DEGREES ANALYZED WITH DIFFERENT AGGREGATE SHAPES AND TEXTURES

To verify the robustness of the angularity characterization based on the virtual cutting method at different angles with different shapes and aggregate textures, four types of aggregates (diabase, gneiss, limestone, and granite) with particle sizes of 16–19 mm were selected to calculate the angularity with Virtual Cutting Method. The numbers of the four types of aggregates were 62, 56, 79, and 92. The 1st and 3rd quartile range values of the box plots for the AI with different aggregates (diabase, gneiss, limestone, and granite) are shown in Table 2. Figure 14(a) shows the data plots and data scatter of the AI values for the diabase aggregates. It can be observed that the shapes of the AI box plots for the angle degrees 1, 3, 5, and 10 are very close to all eight angles in terms of the shapes of the box plots. Figure 14(b) shows the data plots and data scatter of the AI values for the gneiss aggregates. It can be observed that the shapes of the AI box plots for the angle degrees 1, 3, and 5 are very close for all eight angle degrees in terms of the shapes of the box plots. Figure 14(c) shows the data plots and data scatter of the AI values for the limestone aggregates. It can be observed that the shapes of the AI box plots for the angle degrees 1, 3,

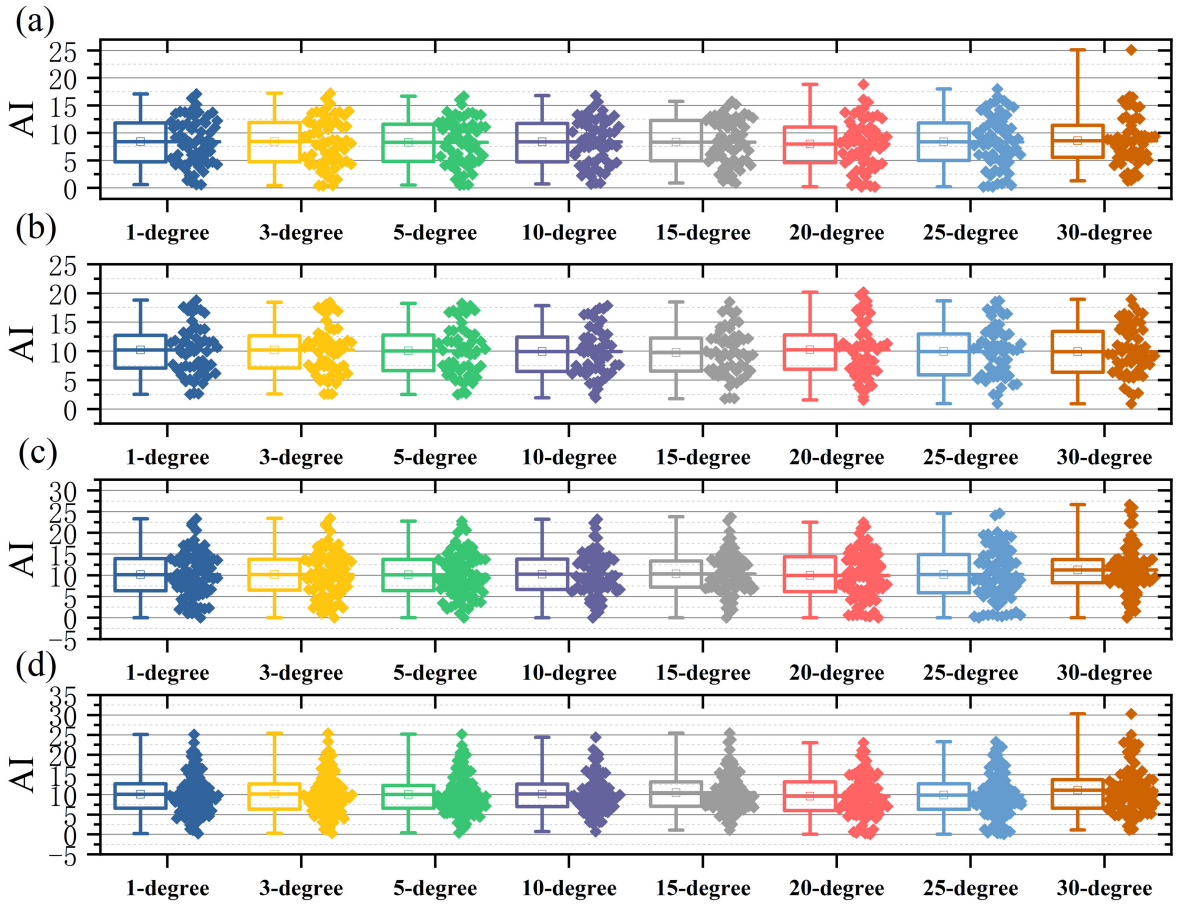

FIGURE 14. Box plots of AI for different textures of aggregates using Virtual Cutting Method: AI for (a) diabase aggregates, (b) gneiss aggregates, (c) limestone aggregates, and (d) granite aggregates.

TABLE 2. AI ranges within first and third quartile ranges of aggregates with different textures using different cutting degrees.

Cutting degrees	Diabase	Gneiss	Limestone	Granite
1	5.17–11.94	7.12–12.86	7.27–14.04	7.38–12.95
3	5.35–11.93	7.15–12.76	7.30–14.03	7.36–12.98
5	5.45-11.59	6.75–12.80	7.27–14.02	7.12–12.83
10	5.57–11.75	6.55–12.55	7.33–14	7.24–12.73
15	5.31–12.32	6.61–12.32	7.59–13.47	7.44–13.32
20	5.03–11.20	6.90–12.83	7.09–14.47	6.80–13.23
25	5.83–11.94	5.97–13.01	6.99–15.33	7.13–13.36
30	5.94–11.87	6.64–13.47	8.26–13.54	7.01–14

5, and 10 are very close for all eight angles in terms of the shapes of the box plots. Figure 14(d) shows the data plots and data scatter of the AI values for the granite aggregates. The shapes of the AI box plots for the angle degrees 1, 3, 5, 10, and 15 are very close for all eight angle degrees in terms of the shapes of the box plots. Similar to the angle degrees analyzed for different size of aggregates (Figure 13), the AI values for the four different aggregates were stable when the angles between two adjacent cutting planes were 1, 3, 5, and 10 degrees, and the 1st and 3rd quartile range values of the box plots for the AI with different aggregates with cutting angle degrees of 1, 3, 5, and 10 are also very close between each other. As seen from Figures 13 and 14, when the angle between two adjacent cutting planes is greater than 10 degrees, the AI value of the four different aggregates become unstable in terms of the shape of the box plots and its data scatter plots. The reason being that with the increase of the cutting angle, fewer intersection contours were extracted for further aggregate AI value calculations, which may not effectively characterize the aggregate angularity. Another reason could be attributed to the fact that the larger angle may miss some important intersection contours, as some of the 3D surfaces that include the key angularity information were not extracted successfully by any cutting planes. It is conceivable that this will affect the accuracy of the aggregate angularity characterization.

3) OPTIMUM ANGLE DEGREE DETERMINATION FOR THE VIRTUAL CUTTING METHOD

As previously discussed, the AI results of angle degrees 1, 3, 5, and 10 are very close (for aggregates with different sizes of aggregates with different shapes or textures). Thus, the next step is to determine the optimum cutting degrees. In our research, the average processing time for single aggregates and the Spearman Correlation Coefficient were calculated to determine the optimum cutting degrees with four types of aggregates, with the sieve size set as 16–19 mm and including diabase, gneiss, limestone, and granite. The average execution times of the Virtual Cutting Method based on the candidate angles (1, 3, 5, and 10 degrees) were calculated for a single particle of the four types of aggregates. As shown in Figure. 15, the execution time decreased when the cutting angle was from 1 to 10 degrees. The main reason being that the smaller the angle, the more intersection contours that can be extracted and more execution time that would be required. It is apparent that the average execution time of the Virtual Cutting Method with the cutting angle (1 degree) is far above the other three options. Therefore, it might be inappropriate to take 1 degree as the virtual cutting angle due to the excessive execution time. For the other three cutting angles (3, 5, and 10 degrees), the average execution time was 49.993, 33.264, and 18.4 ms, respectively. Compared with the cutting angle of 1 degree, the difference in the execution time is relatively small.

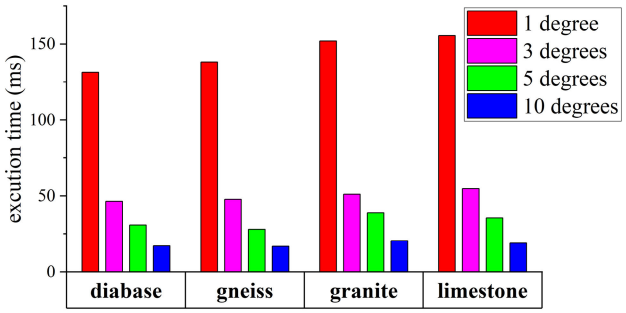

FIGURE 15. Average execution time of Virtual Cutting Method with different cutting degrees for aggregates (diabase, gneiss, granite and limestone) with different textures.

In order to determine the optimum angle, the Spearman Correlation Coefficient was calculated. The Spearman Correlation Coefficient is defined by the following equation:

$$\rho = \frac{\sum_{i=1}^{n} (x_i - \bar{x})\,(y_i - \bar{y})}{\sqrt{\sum_{i=1}^{n} (x_i - \bar{x})^2 - \sum_{i=1}^{n} (y_i - \bar{y})^2}} \tag{7}$$

where n is the sample size for the four aggregates (diabase, gneiss, limestone, and granite), x represents the AI value that was calculated using the Virtual Cutting Method with cutting angles of 3, 5 and 10 degrees, and y represents the AI value with the cutting angle as 1 degree. The Spearman Correlation Coefficient has a value from −1 to 1 and the value zero indicates that there is no relevance between x and y. By contrast, a value close to 1 shows a monotonically related relationship between x and y. Thus, it could be concluded that the higher the calculated Spearman Correlation Coefficient, the closer the angularity characterization ability of the Virtual Cutting Method with the given cutting angle approach (with a cutting angle of 1 degree). Table 3 shows the Spearman Correlation Coefficient of the cutting angles of 3, 5 and 10 degrees with that of 1 degree.

It can be found that that the average Spearman Correlation Coefficient of the 3 and 5 degrees cutting angles were very close to each other, and both are above 99.5%, indicating that the AI results of the angle degrees of 3 and 5 have a strong correlation with that of angle degree 1. By contrast, the average Spearman The correlation coefficient of the 10-degree cutting angle was 97% and was not stable for the four kinds of aggregates(from 94% to 97%). Practically, the optimum angle can be selected by considering the trade-off between accuracy and run-time. From the results, it can be observed that the AI results of the 5-degree cutting angle were accurate and robust for the four kinds of aggregates under acceptable average processing times. Thus, the 5-degree cutting angle was selected as the optimal cutting degree in the current research.

TABLE 3. Correlation matrix for AI of 1 degree with AI of 3, 5 and 10 degrees.

Aggregate	3 degrees	5 degrees	10 degrees
diabase	0.998388	0.995316	0.971695
gneiss	0.998086	0.997129	0.995625
limestone	0.998247	0.996154	0.966188
granite	0.997858	0.995777	0.945671

B. COMPARING THE VIRTUAL CUTTING METHOD WITH THE 2D AND 3D PROJECTION METHOD

To determine the validity of the proposed virtual cutting method, the AI results of the method were compared with the 2D and 3D projection methods based on the gradient approach mentioned previously. The following procedure was adopted: (a) the analysis of variance (ANOVO) test was used to determine the differences in the results of the three methods of testing for the angularity of the aggregates of diabase, gneiss, limestone, and granite; (b) comparing the angularity calculated by the Virtual Cutting Method and the gradient method using 2D/3D projection images.

1) THE ANOVO TEST FOR DIFFERENT AGGREGATES

ANOVO test was used to compare several groups of observations that were independent and may have a different mean. Since the AI for angularity was defined in different terms, the angularity characteristics cannot be directly compared with each other using ANOVO analysis. In general, the four kinds of aggregates (diabase, gneiss, limestone, and granite) might differ in angularity. Thus, if an angularity characterization method can distinguish between the lithologies,

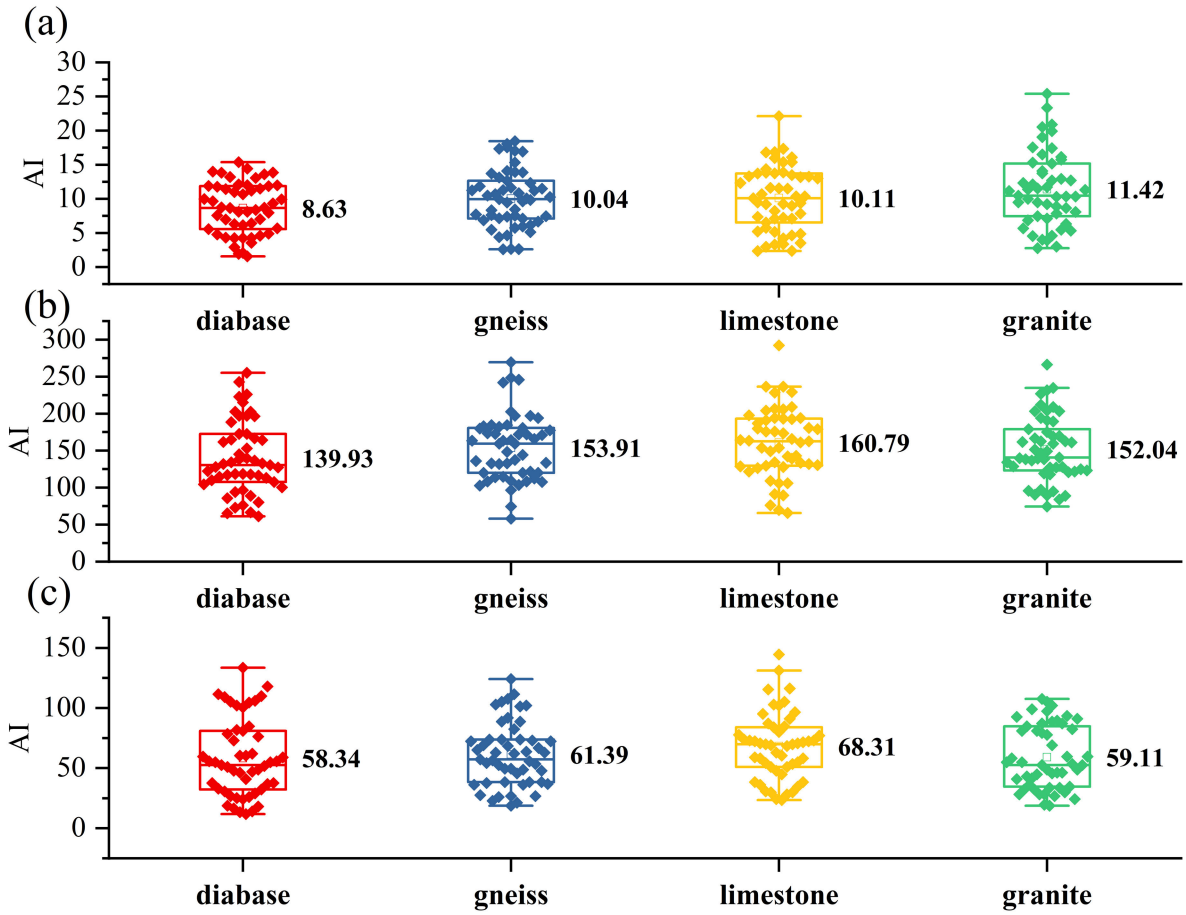

FIGURE 16. Box plots of AI using different methods for different textures of aggregates: AI using (a) Virtual Cutting Method, (b) 2D projection method, and (c) 3D projection method.

it can be regarded as an effective method. The ANOVO tests reported herein were used to determine whether the differences between the four aggregates were significant for angularity characterization. 50 particles of each aggregate type were randomly selected to calculate the AI using the Virtual Cutting Method and the gradient method using 2D/3D projection images. In addition, the Tukey Multiple Compare test was performed based on the python statistics module named 'statsmodels'.

Table 4 shows the method groups for the ANOVO test, whereas Table 5 shows the ANOVO test results. The test is as follows: H_0(in which $u_1 = u_2 = u_3$) versus H_a(in which at least one mean differs), where u_1,u_2, and u_3 are the AI values calculated using the Virtual Cutting Method and the 2D and 3D Projection Methods, respectively. Setting α =0.05, we rejected H_0 if p value$< \alpha$. The p-values of three methods for distinguishing each pair of materials are shown in Table 5. It can be observed that the only significant result that one can obtain is to distinguish diabase and granite using the proposed Virtual Cutting Method (p=0.01). In addition to this observation, none of the other methods can provide reliable results for distinguishing any two kinds of materials. This proves the usability of the Virtual Cutting method, though a limitation exists that needs additional optimization.

TABLE 4. Group definitions for ANOVO test.

Aggregate	Group
diabase	1
gneiss	2
limestone	3
granite	4

2) COMPARING THE AI OF DIFFERENT AGGREGATES BASED ON THE THREE METHODS

Figure 16 plots the AI boxplots for the four kinds of aggregates (diabase, gneiss, limestone, and granite) using the Virtual Cutting, 2D, and 3D Projection methods. Notably, 50 particles of each aggregate type were randomly selected to calculate the AI using the Virtual Cutting Method and the gradient method using 2D/3D projection images. By analyzing the mean value of the AI for different aggregates, the AI ranking can be acquired for different aggregates. It can be

TABLE 5. ANOVO results of Virtual Cutting and 2D/3D projection methods.

Group1	Group2	p value of ANOVO test for different groups		
		Virtual cutting	2D projection	3D projection
diabase	gneiss	0.49	0.55	0.43
diabase	granite	**0.01**	0.76	0.55
diabase	limestone	0.45	0.07	0.11
gneiss	granite	0.42	0.9	0.9
gneiss	limestone	0.90	0.63	0.87
granite	limestone	0.47	0.40	0.75

TABLE 6. First quartile (Q1), median (Q2) and third quartile (Q3) of AI calculated using Virtual Cutting Method and 2D/3D projection methods.

Aggregates	Virtual cutting			2D projection			3D projection		
	Q1	Q2	Q3	Q1	Q2	Q3	Q1	Q2	Q3
diabase	5.57	8.69	11.88	32.30	53.80	80.90	107.60	131.62	172.79
gneiss	7.10	10.00	12.63	38.48	59.69	73.83	120.17	159.44	180.64
limestone	6.52	10.23	13.71	51.05	69.90	84.04	129.59	162.97	193.21
granite	7.44	10.82	15.16	34.56	53.01	84.82	123.30	143.72	179.07

seen from Figure 16(a) that the AI ranking for the four kinds of aggregates using the Virtual Cutting Method from low to high is as follows: diabase, gneiss, limestone, and granite. Based on Figure 16(b) and (c), it can be seen that the AI ranking of different aggregates for the 2D and 3D Projection Methods are the same, that is diabase, granite, gneiss, and limestone. Therefore, for the aggregates diabase, gneiss and limestone, the angularity characterization results of the three methods are consistent; the limestone aggregates are the most angular, the gneiss aggregates are the second-most angular, and the diabase aggregates are the least-angular. However, the AI ranking order for the granite aggregates is different in the four kinds of aggregates using the three AI evaluation methods. The granitic aggregates are the most angular when using the Virtual Cutting Method (Figure 16a), and they are the second least angular using the 2D (Figure 16b) and 3D Projection methods (Figure 16c). One of the reasons for this interpretation might be that the sampled granite aggregates have a more uneven surface compared with the other three aggregates. In addition, to obtain accurate projection images of aggregates on the XY plane in the XYZ coordinate system, the aggregates were non-touched while capturing images. This can ensured that the projection contour on the XY plane and most of the contour points on the XZ and YZ planes, were extracted accurately even if the threshold segmentation method was used. Thus, the AI ranking results calculated using the 2D/3D projection methods are reliable despite some fake edges existing in the 3D projection method. Taken together, these results showed that the proposed Virtual Cutting Method can be used to characterize the angularity of aggregates based on the top surface of the 3D objects.

For further evaluating the effectiveness of the Virtual Cutting Method, the AI ranking lists of the first quartile (Q1), median (Q2) and third quartile (Q3) for the four kinds of aggregates using the three methods were compared. The AIs of Q1, Q2 and Q3 for the four kinds of aggregates are presented in Table 6. Further analysis from Table 6 and Figure 16 showed that, for the Virtual Cutting Method and 3D Projection method, the AI ranking lists (from low to high) of Q2 and Q3 are the same as the ranking order of the AI mean value. Furthermore, the AI ranking of Q1 is slightly different from the mean value. For the 2D projection method, only the AI ranking order (from low to high) of Q1 is the same as the order of the mean value. Thus, it can be concluded that the AI characterization method based on the 3D information was robust in the distribution of data. The reason for this might be because the 3D information of aggregates can be more objective in the characterization of angularity.

V. CONCLUSION

The aim of this paper was to evaluate the AI of aggregates on conveyor belts based on 3D upper-side point cloud images. A new method named the ''Virtual Cutting Method'' was proposed in the current research. First, we created a set of virtual planes with equal angle-intervals between two neighboring planes to extract contour lines from the triangularized 3D surface of the aggregate. The AI of the aggregate was then calculated by the gradient method used in AIMS2 systems. In addition, a procedure for determining the optimum degrees of the Virtual Cutting Method was proposed in terms of accuracy and execution time. Furthermore, we performed ANOVO tests on the AIs of the Virtual Cutting, 2D, and 3D projection methods for different aggregates, and also compared the ranking order of AI in terms of mean value, first quartile (Q1), median (Q2) and third quartile (Q3) using the three methods for different aggregates. In summary, the results indicate that the AI results of the three methods were consistent, even though there were some differences for the granitic aggregates. In addition, the AI ranking order of the Virtual Cutting method was relatively more stable than those of the 2D projection method with respect to the mean and quartile values. Taken together, these findings demonstrate the practicability and validity of the Virtual Cutting method and suggest that it can be used to evaluate the angularity of aggregates by relying on the partial 3D information. Moreover, the proposed method does not require the complete projection contour of the aggregate particle image. The proposed method can be applied for the angularity

characterization of coarse aggregates regardless of whether aggregates are separated or in piles while capturing images, which makes this method a good candidate for measuring the AI of aggregates on conveyor belts. In the future, we will focus on reducing the execution time of the AI evaluation using the Virtual Cutting Method, to enable it to be used for the angularity characterization of aggregates on conveyor belts in real-time.

REFERENCES

[1] W. Sun, L. Wang, and E. Tutumluer, "Image analysis technique for aggregate morphology analysis with two-dimensional Fourier transform method," *Transp. Res. Rec., J. Transp. Res. Board*, vol. 2267, no. 1, pp. 3–13, Jan. 2012.

[2] L. Wang, W. Sun, E. Tutumluer, and C. Druta, "Evaluation of aggregate imaging techniques for quantification of morphological characteristics," *Transp. Res. Rec., J. Transp. Res. Board*, vol. 2335, no. 1, pp. 39–49, Jan. 2013.

[3] P. Polaczyk, X. Shu, H. Gong, and B. Huang, "Influence of aggregates angularity on the locking point of asphalt mixtures," *Road Mater. Pavement Design*, vol. 20, no. sup1, pp. S183–S195, Apr. 2019.

[4] S. J. Lee, C. H. Lee, M. Shin, S. Bhattacharya, and Y. F. Su, "Influence of coarse aggregate angularity on the mechanical performance of cement-based materials," *Construct. Building Mater.*, vol. 204, pp. 184–192, Apr. 2019.

[5] C. Rao, E. Tutumluer, and I. T. Kim, "Quantification of coarse aggregate angularity based on image analysis," *Transp. Res. Record, J. Transp. Res. Board*, vol. 1787, no. 1, pp. 117–124, Jan. 2002, doi: 10.3141/1787-13.

[6] D. Zhang, X. Huang, and Y. Zhao, "Investigation of the shape, size, angularity and surface texture properties of coarse aggregates," *Construct. Building Mater.*, vol. 34, pp. 330–336, Sep. 2012.

[7] J. Gao, H. Wang, Y. Bu, Z. You, M. R. M. Hasan, and M. Irfan, "Effects of coarse aggregate angularity on the microstructure of asphalt mixture," *Construct. Building Mater.*, vol. 183, pp. 472–484, Sep. 2018, doi: 10.1016/j.conbuildmat.2018.06.170.

[8] Z. Tong, J. Gao, and H. Zhang, "Innovation for evaluating aggregate angularity based upon 3D convolutional neural network," *Construct. Building Mater.*, vol. 155, pp. 919–929, Nov. 2017.

[9] E. Masad, *Test Methods for Characterizing Aggregate Shape, Texture, and Angularity*. Washington, DC, USA: Transportation Research Board, 2007.

[10] J. Yang and S. Chen, "An online detection system for aggregate sizes and shapes based on digital image processing," *Mineralogy Petrology*, vol. 111, no. 1, pp. 135–144, Feb. 2017.

[11] R. Cao, Y. Zhao, Y. Gao, X. Huang, and L. Zhang, "Effects of flow rates and layer thicknesses for aggregate conveying process on the prediction accuracy of aggregate gradation by image segmentation based on machine vision," *Construct. Building Mater.*, vol. 222, pp. 566–578, Oct. 2019.

[12] H. Yaghoobi, H. Mansouri, M. A. E. Farsangi, and H. Nezamabadi-Pour, "Determining the fragmented rock size distribution using textural feature extraction of images," *Powder Technol.*, vol. 342, pp. 630–641, Jan. 2019.

[13] S. Zhang, R. Li, and J. Pei, "Evaluation methods and indexes of morphological characteristics of coarse aggregates for road materials: A comprehensive review," *J. Traffic Transp. Eng., English Ed.*, vol. 6, no. 3, pp. 256–272, Jun. 2019.

[14] B. Zhang, S. J. Lee, Y. Qian, E. Tutumluer, and S. Bhattacharya, "A smartphone-based image analysis technique for ballast aggregates," in *Proc. Int. Conf. Transp. Develop.*, Jun. 2016, pp. 623–630.

[15] G. Christie, K. Kochersberger, and A. L. Abbott, "Fast inspection for size-based analysis in aggregate processing," *Mach. Vis. Appl.*, vol. 26, no. 1, pp. 31–40, Jan. 2015.

[16] H. Rahmani, C. Scanlan, U. Nadeem, M. Bennamoun, and R. Bowles, "Automated segmentation of gravel particles from depth images of gravel-soil mixtures," *Comput. Geosci.*, vol. 128, pp. 1–10, Jul. 2019.

[17] I. C. Engin and N. H. Maerz, "Size distribution analysis of aggregates using LiDAR scan data and an alternate algorithm," *Measurement*, vol. 143, pp. 136–143, Sep. 2019.

[18] I. C. Engin, "Comparison of the different mathematical methods performed in determining the size distribution of aggregates using LiDAR point cloud data and suggested algorithm," *Earth Sci. Informat.*, vol. 12, no. 3, pp. 365–380, 2019.

[19] Q. Wang, Y. Tan, and Z. Mei, "Computational methods of acquisition and processing of 3D point cloud data for construction applications," *Arch. Comput. Methods Eng.*, vol. 27, no. 2, pp. 479–499, Apr. 2020.

[20] S. Zhang, "High-speed 3D shape measurement with structured light methods: A review," *Opt. Lasers Eng.*, vol. 106, pp. 119–131, Jul. 2018.

[21] R. Szeliski, *Computer Vision: Algorithms and Applications*. London, U.K.: Springer, 2010.

[22] F. Remondino and S. El-Hakim, "Image-based 3D modelling: A review," *Photogramm. Rec.*, vol. 21, no. 115, pp. 269–291, Aug. 2006.

[23] D. Moon, S. Chung, S. Kwon, J. Seo, and J. Shin, "Comparison and utilization of point cloud generated from photogrammetry and laser scanning: 3D world model for smart heavy equipment planning," *Autom. Construct.*, vol. 98, pp. 322–331, Feb. 2019.

[24] S. Zhang and S.-T. Yau, "Three-dimensional shape measurement using a structured light system with dual cameras," *Opt. Eng.*, vol. 47, no. 1, 2008, Art. no. 013604, doi: 10.1117/1.2835686.

[25] H. Kim, "Automation of aggregate characterization using laser profiling and digital image analysis," Ph.D. dissertation, Dept. CAEE., UT Austin Univ., Austin, TX, USA, 2002.

[26] Y. Guo, V. Markine, X. Zhang, W. Qiang, and G. Jing, "Image analysis for morphology, rheology and degradation study of railway ballast: A review," *Transp. Geotechnics*, vol. 18, pp. 173–211, Mar. 2019.

[27] E. Masad and T. Fletcher, "Aggregate imaging system (AIMS): Basics and applications," Texas Transp. Inst., Austin, TX, USA, Tech. Rep. FHWA/TX-05/5-1707-01-1, Oct. 2005.

[28] S. L. Palasamudram and S. Bahadur, "Particle characterization for angularity and the effects of particle size and angularity on erosion in a fluidized bed environment," *Wear*, vols. 203–204, pp. 455–463, Mar. 1997.

[29] Y. Descantes, Y. Fosse, and F. Milcent, "Automated measurement of railway ballast angularity," *J. Mater. Civil Eng.*, vol. 18, no. 4, pp. 612–618, Aug. 2006.

[30] M. Moaveni, S. Wang, J. M. Hart, E. Tutumluer, and N. Ahuja, "Evaluation of aggregate size and shape by means of segmentation techniques and aggregate image processing algorithms," *Transp. Res. Rec., J. Transp. Res. Board*, vol. 2335, no. 1, pp. 50–59, Jan. 2013.

[31] N. H. Maerz, "Technical and computational aspects of the measurement of aggregate shape by digital image analysis," *J. Comput. Civil Eng.*, vol. 18, no. 1, pp. 10–18, Jan. 2004.

[32] S. J. Blott and K. Pye, "Particle shape: A review and new methods of characterization and classification," *Sedimentology*, vol. 55, no. 1, pp. 31–63, 2008.

[33] E. Mahmoud, L. Gates, E. Masad, S. Erdoğan, and E. Garboczi, "Comprehensive evaluation of AIMS texture, angularity, and dimension measurements," *J. Mater. Civil Eng.*, vol. 22, no. 4, pp. 369–379, Apr. 2010.

[34] T. Al-Rousan, E. Masad, E. Tutumluer, and T. Pan, "Evaluation of image analysis techniques for quantifying aggregate shape characteristics," *Construct. Building Mater.*, vol. 21, no. 5, pp. 978–990, May 2007.

[35] L. Wang, X. Wang, L. Mohammad, and C. Abadie, "Unified method to quantify aggregate shape angularity and texture using Fourier analysis," *J. Mater. Civil Eng.*, vol. 17, no. 5, pp. 498–504, Oct. 2005.

[36] A. du Plessis and W. P. Boshoff, "A review of X-ray computed tomography of concrete and asphalt construction materials," *Construct. Building Mater.*, vol. 199, pp. 637–651, Feb. 2019.

[37] E. Masad, S. Saadeh, T. Al-Rousan, E. Garboczi, and D. Little, "Computations of particle surface characteristics using optical and X-ray CT images," *Comput. Mater. Sci.*, vol. 34, no. 4, pp. 406–424, Dec. 2005.

[38] C. Jin, X. Yang, Z. You, and K. Liu, "Aggregate shape characterization using virtual measurement of three-dimensional solid models constructed from X-ray CT images of aggregates," *J. Mater. Civil Eng.*, vol. 30, no. 3, Mar. 2018, Art. no. 04018026.

[39] J. Wu, L. Wang, Y. Hou, H. Xiong, Y. Lu, and L. Zhang, "A digital image analysis of gravel aggregate using CT scanning technique," *Int. J. Pavement Res. Technol.*, vol. 11, no. 2, pp. 160–167, Mar. 2018.

[40] X. Yang, S. Chen, and Z. You, "3D voxel-based approach to quantify aggregate angularity and surface texture," *J. Mater. Civil Eng.*, vol. 29, no. 7, Jul. 2017, Art. no. 04017031.

[41] S. T. Erdogan, P. N. Quiroga, D. W. Fowler, H. A. Saleh, R. A. Livingston, E. J. Garboczi, P. M. Ketcham, J. G. Hagedorn, and S. G. Satterfield, "Three-dimensional shape analysis of coarse aggregates: New techniques for and preliminary results on several different coarse aggregates and reference rocks," *Cement Concrete Res.*, vol. 36, no. 9, pp. 1619–1627, Sep. 2006.

[42] E. Tutumluer, D. Mishra, and A. A. Butt, "Characterization of Illinois aggregates for subgrade replacement and subbase," Illinois Center Transp., Urbana, IL, USA, Tech. Rep. FHWA-ICT-09-060, 2009.
[43] H. Kim, C. T. Haas, A. F. Rauch, and C. Browne, "Wavelet-based three-dimensional descriptors of aggregate particles," *Transp. Res. Rec., J. Transp. Res. Board*, vol. 1787, no. 1, pp. 109–116, Jan. 2002.
[44] J. R. J. Lee, M. L. Smith, and L. N. Smith, "A new approach to the three-dimensional quantification of angularity using image analysis of the size and form of coarse aggregates," *Eng. Geol.*, vol. 91, nos. 2–4, pp. 254–264, May 2007.
[45] T. Pan and E. Tutumluer, "Evaluation of visual based aggregate shape classifications using the university of illinois aggregate image analyzer (UIAIA)," in *Proc. Pavement Mech. Perform.*, May 2006, pp. 203–211.
[46] Y. Gao and Q. Dai, "View-based 3D object retrieval: Challenges and approaches," *IEEE MultimediaMag.*, vol. 21, no. 3, pp. 52–57, Jul. 2014.
[47] R. Haralick, "Pose estimation from corresponding point data," *Mach. Vis. Inspection Meas.*, vol. 19, no. 6, pp. 1–84, 1989.
[48] L. Technologies. *15159-5.2.18.11_MANUAL_User_Gocator_Line_Profile_Sensors*. Accessed: Sep. 5, 2019. [Online]. Available: https://downloads.lmi3d.com/gocator-line-profile-sensors-user-manual-version-454102
[49] D. D. Morris and T. Kanade, "Image-consistent surface triangulation," in *Proc. IEEE Conf. Comput. Vis. Pattern Recognit. CVPR*, Jun. 2000, pp. 332–338.
[50] M. S. GmbH. <*solution_guide_iii_c_3d_vision*>. Accessed: Oct. 10, 2019. [Online]. Available: http://download.mvtec.com/halcon-9.0-solution-guide-iii-c-3d-vision.pdf

HANYE LIU (Member, IEEE) received the master's degree from Xidian University. He is currently pursuing the Ph.D. degree with the School of Information Engineering, Chang'an University, Xi'an, China. He is also an Associate Professor with the School of Information Engineering, Yulin University, Yulin, China. His current research interests include aggregates particle characterization, 3D point cloud image processing, and machine leaning application.

ZHAOYUN SUN received the M.S. degree in computer application from Xi'an Highway University, in 1991, and the Ph.D. degree in road and railway engineering from Chang'an University, in 2007. She has been a Professor with the Department of Electronic Information, Chang'an University, since 2003. Her research interests include intelligent traffic condition detection and information processing, digital image processing, and traffic information engineering and control.

WEI LI received the B.S. and M.S. degrees in optoelectronic technique from Xidian University, China, in 2003 and 2006, respectively, and the Ph.D. degree in physical electronics from the University of Chinese Academy of Sciences, Xi'an, China, in 2009. His research interests include digital image processing, automatic pavement condition detection and evaluation, machine learning, deep learning, and so on.

JU HUYAN received the B.Sc. and M.Sc. degrees from Chang'an University, Xi'an, China. She is currently working as a Postdoctoral Fellow at the Centre for Pavement and Transportation Technology (CPATT). She joined CPATT, in 2016. Her current research interests include pavement management; pavement condition evaluation; 3D (2D) image processing pavement distress detection; and artificial intelligent (AI), machine learning, and deep learning techniques for pavement condition assessment and evaluation.

MENG GUO received the Ph.D. degree in highway and railway engineering from the Harbin Institute of Technology. He is currently a Professor with the Beijing University of Technology. He has published 64 publications in refereed journals and conference proceedings. The H-index is 18 in Google Scholar. His current research interests include evaluating fundamental properties related to the interfacial interaction between asphalt binder and mineral aggregate, the characterization of physio-chemical properties of aggregates and asphalt binders, and the efficient use of additives to improve performance of asphalt mixtures.

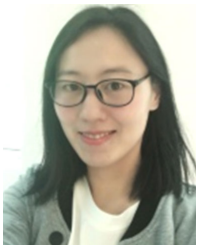

XUELI HAO was born in Shandong, China, in 1987. She received the Ph.D. degree in traffic information engineering and control from Chang'an University, Xi'an, China, in 2015. She is currently a Senior Engineer with the School of Information Engineering, Chang'an University. Her current research interests include pavement materials property analysis and pavement performance detection.